

Article

Ablation-Dominated Arcs in CO₂ Atmosphere - Part I: Temperature Determination near Current Zero

Ralf Methling^{1,†} , Alireza Khakpour^{1,†} , Nicolas Götte^{2,†} , and Dirk Uhrlandt^{1,†} 

¹ Leibniz Institute for Plasma Science and Technology (INP), Felix-Hausdorff-Str. 2, 17489 Greifswald, Germany; methling@inp-greifswald.de

² Institute for High Voltage Technology, RWTH Aachen University, Schinkelstrasse 2, 52056 Aachen, Germany; e-mail@e-mail.com

* Correspondence: methling@inp-greifswald.de; Tel.: +49-3834-554-3840

† These authors contributed equally to this work.

Abstract: Wall-stabilized arcs dominated by nozzle-ablation are key elements of self-blast circuit breakers. In the present study, high-current arcs were investigated using a model circuit breaker (MCB) in CO₂ as gas alternative to SF₆ and in addition a long polytetrafluoroethylene nozzle under ambient conditions for stronger ablation. The assets of different methods for optical investigation were demonstrated, e.g. high-speed imaging with channel filters and optical emission spectroscopy. Particularly the phase near current zero (CZ) crossing was studied in two steps. In the first step using high-speed cameras, radial temperature profiles have been determined until 0.4 ms before CZ in the nozzle. Broad temperature profiles with a maximum of 9400 K have been obtained from analysis of fluorine lines. In the second step, the spectroscopic sensitivity was increased using an intensified CCD camera, allowing single-shot measurements until few microseconds before CZ in the MCB. Ionic carbon and atomic oxygen emission were analyzed using absolute intensities and normal maximum. The arc was constricted and the maximum temperature decreased from >18000 K at 0.3 ms to about 11000 K at 0.010 ms before CZ. The arc plasma needs about 0.5-1.0 ms after both the ignition phase and the current zero crossing to be completely dominated by the ablated wall material.

Keywords: circuit breaker; switching arc; optical emission spectroscopy; ablation; current zero; SF₆ alternative gases; CO₂; PTFE

1. Introduction

For modern power transmission and distribution grids, high voltage circuit breakers are among the essential elements to ensure safe power flow [1,2]. A basic technology applied therefore are self-blast circuit breakers in which a pressure build-up in a heating volume, necessary for arc quenching around current zero (CZ), is produced by the ablation of material from the nozzle wall due to intense arc radiation. Usually, gas sulfur hexafluoride (SF₆) is applied as quenching and insulating gas due to its unique properties as being chemically inert, non-flammable, non-explosive, non-toxic, thermally stable, and an excellent electrical insulator and arc interrupter due to its high electronegativity (electron attachment) and density [3]. Metal-doped polytetrafluoroethylene (PTFE) is used as the nozzle material due to well-adjustable ablation, pressure built-up, and dielectric properties. A main trend of circuit breaker development is the substitution of the extremely potent greenhouse gas SF₆ with a high global warming potential (of about 23000 times that of CO₂ over a 100 year period) by more environment-friendly gases [4]. A variety of alternative gases has been discussed and tested in the last decades, e.g. CO₂, CF₃I, C₂F₄, c-C₄F₈, C₄F₇N, and C₅F₁₀ as pure gases or in a mixtures of two or three gases including components like N₂, O₂, and CO₂. However, only a limited

32 selection remains in the actual investigations. Gas mixtures containing fluoro–nitriles (C_4F_7N) or
33 fluoro–ketones ($C_5F_{10}O$) as minority components (<20 %) have been identified as most promising
34 alternatives to SF_6 in high–voltage gas–insulated switchgear applications, because of their low global
35 warming potential together with their dielectric strength values being comparable to SF_6 [5–7]. Due to
36 high boiling points (at 1 bar) of the fluoro–ketones (27°C) and fluoro–nitriles (–4.7°C), gas mixtures
37 with carbon dioxide CO_2 as buffer gas prevent liquefaction at temperatures below –30°C. One of the
38 most promising alternatives that has less limitations concerning temperature range and greenhouse
39 effect but reasonable electrical insulation is CO_2 [8–10]. Moreover, some of the experimental techniques
40 and results obtained for CO_2 will be relevant for other alternative gases that are usually applied with
41 CO_2 as buffer gas.

42 For an evaluation of the interruption performance it is mandatory to analyze and understand
43 the time around CZ, i.e. the phase of current interruption and recovery of dielectric insulation in the
44 electrode gap. Beside experimental investigations, computer simulations are of high importance due to
45 their cost–efficiency and fast adaptation to different geometries. However, such simulation tools need
46 to be validated with experimental results and also to be provided with reliable input parameters based
47 on experimental data. From the physical point of view, numerous transient effects can be observed
48 such as

- 49 • reversal of the gas flow in the heating channel,
- 50 • transition from an ablation–controlled to an axially blown arc,
- 51 • arc constriction and finally extinction,
- 52 • wall ablation that still occurs when the energy input by radiation from the arc is terminated, and
- 53 • dielectric recovery of the electrode gap region.

54 Hence, the experimental investigation of the CZ phase is of high relevance for the development of high
55 voltage switchgear. One of the main goals is the determination of physical properties as composition,
56 pressure and temperature of the plasma. Ideally, this should be done with both spatial and temporal
57 resolution as close as possible to CZ. Such investigations are usually based on optical methods and
58 demand view ports or other access to the arc plasma that is often not available for commercial circuit
59 breakers. A balance must be found between a conservation of geometry, functionality, and plasma
60 conditions on the one side and a modification of the setup on the other side allowing, e.g., optical access
61 as well as fast exchange of fill gas and components as electrodes, nozzles, windows, and ignition wires.
62 In general, model circuit breakers are often equipped with fixed electrodes and ignited by explosion
63 of thin wires [11]. Experiments with moving electrodes of pin and tulip shape may provide higher
64 similarity with commercial circuit breaker geometries including the geometry of nozzles, heating
65 chambers, and gas flow. However, reproducibility is often critical for experiments with moving
66 electrodes. Furthermore, often the optical access is either fairly sophisticated and limited in time (using
67 slits and windows [12]) or limited in spatial resolution, e.g. using optical fibers. If side–on diagnostics
68 of the arc through quartz windows placed outside the nozzle is not possible due to non–transparent
69 vapor, an alternative end–on arc observation can be realized through a ring electrode [13]. Alternatively,
70 the PTFE as the standard nozzle material in commercial circuit breakers can be replaced by polymers
71 that are transparent, e.g. PMMA [14,15].

72 In this work, two setups are used for investigation with optical emission spectroscopy (OES).
73 In both setups, two pin electrodes are placed in a fixed distance and surrounded by PTFE nozzles.
74 Ignition wires are used to initiate the arcs. The main difference between the setups is the nozzle
75 geometry:

- 76 • The first, more simple setup is applied to generate extra–high pressure built–up and strong
77 influence of the wall ablation. Therefore, the nozzle is made of a single, long PTFE tube. The
78 influence of ignition wire and surrounding gas (ambient air) during the early stage of the arc
79 discharge have been investigated in [16]. In the present work, the focus is set on the gas flow
80 reversal as well as the detection limits for the determination of plasma temperature profiles
81 around CZ. For these issues, no surrounding chamber is needed.

82 • The second setup is a model self-blast circuit breaker in a CO₂ atmosphere with optical access
83 via windows. It consists of two nozzles surrounding the electrodes and forming a heating
84 channel which leads into the heating volume. Earlier experiments were carried out with the
85 optical observation at the position of the heating channel and in the high-current phase [17].
86 Hence, the plasma emission from the central parts of the arc is influenced by the axial flow
87 of hot gas in the heating channel, i.e. along the line of sight. The gas flow into the heating
88 volume partly forces the plasma into the heating channel, and the emission region exceeds the
89 nozzle diameter, showing turbulence and deviation from the expected bi-convex structure that is
90 needed for plasma temperature determination. To overcome these problems, for the experiments
91 reported here the observation position was shifted away from the heating channel and towards
92 the electrodes. As described below, this was realized by insertion of quartz windows into the
93 nozzles.

94 For the investigation of the arc plasma, OES of atomic and ionic lines is a standard method for
95 experimental determination of temporally and spatially resolved profiles of composition, temperature,
96 and partial pressures that are needed for the calculation of thermal and electrical conductivity. However,
97 the applicability of optical emission spectroscopy is limited for low emission levels, e.g. at low currents
98 around CZ or at positions near the nozzle wall. Usually, plasma temperatures below 8000 K cannot be
99 measured due to low line intensity and limited sensitivity of the detector. Thus, spatial temperature
100 profiles cannot be obtained in the close vicinity of the wall region that is of high interest due to
101 importance of the nozzle ablation [18,19].

102 However, at reduced temperatures the majority of atoms is in the ground state and could be
103 analyzed by optical absorption spectroscopy (OAS) of resonant lines. Nevertheless, resonant lines
104 of the relevant species are in the ultraviolet (UV) wavelength region (C, F, Cu) that is difficult to
105 investigate under switching-relevant conditions and demands a lot of technical effort. Many other lines
106 are very weak (O I at 630.03 nm). An alternative to the investigation of atomic and ionic lines is the
107 spectroscopic investigation of molecules. Most molecules dissociate above critical temperatures below
108 10000 K. They may provide insight into the region close to the wall at lower temperature. Experiments
109 on OAS and investigation of molecule emission and absorption are reported in an accompanying
110 article [20].

111 In the present paper, several questions should be answered: What can be learned by application
112 of different experimental techniques for instigation of ablation-dominated arcs, partly combined?
113 How far to current zero plasma temperature profiles can be measured with OES? What happens in the
114 low-current phase approaching CZ with these profiles when lower conductivities are needed - mainly
115 a temperature decrease or constriction of the arc diameter?

116 2. Materials and Methods

117 2.1. Geometry of electrodes and nozzles

118 As described above, two setups of electrodes and nozzles are used. They are sketched in Figure 1.
119 In both cases, two pin tungsten-copper (W-Cu) electrodes of 10 mm diameter were placed horizontally
120 with a fixed contact distance of 40 mm. The electrodes were surrounded by either one 126 mm long,
121 tubular shaped nozzle of 50 mm outer diameter (a) or two separate nozzles of about 50 mm length
122 and 104 mm outer diameter (b). The general structure of the tubular and the separated nozzles were
123 similar. They were made of PTFE doped with <0.5 wt % molybdenum disulfide (MoS₂) as usually used
124 in high-voltage CBs. In both cases, the inner diameter was about 12 mm in the central part where the
125 arc discharge was burned and about 16 mm at the electrode side ends of the nozzle to allow an exhaust
126 gas flow along the electrodes. In the vicinity of the electrode tips, a smooth transition was realized
127 from the smaller to the larger diameter.

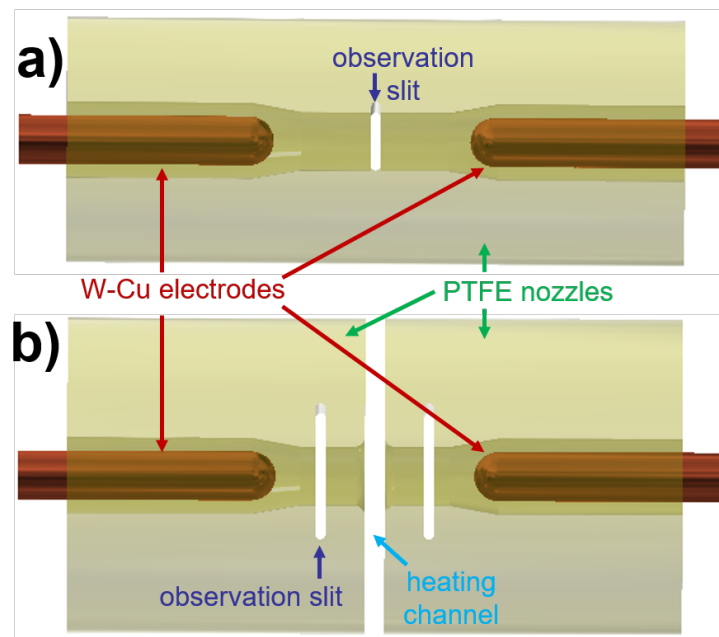


Figure 1. Setups (a) with a closed, long PTFE nozzle for experiments with strong ablation and high pressure built-up and vertical observation slits in the middle and (b) with two separated PTFE nozzles forming a heating channel for plasma flow into a heating volume as used for the model circuit breaker.

128 For the camera observation and spectroscopy, optical access was realized by vertical slits of 2 mm
 129 width. Pairwise placement at opposite positions allowed not only observation of the emitted radiation
 130 but also background illumination and absorption measurement. The slits were mortised directly into
 131 the nozzles, ranging over the complete nozzle diameter. Since such slits would be potential exhaust
 132 pipes of the plasma causing additional disturbances, 2 mm-thick quartz plates were applied to seal
 133 the nozzle. After each shot the sealing plates were checked visually; the transmission was measured
 134 regularly. Because of the possible fume deposition on the plates, they were exchanged after each shot
 135 but could be recycled after cleaning. Generally, it was found that the sealing was very effective and
 136 the transmission reduction was controllable; however, few cases were observed with severe, local
 137 blackening of the quartz plates indicating problems with the sealing. Breaking of the plates occurred
 138 only ones after extremely high currents.

139 For setup (a) the observation slits were placed in the middle between both electrodes, i.e. about
 140 20 mm away from both electrodes. In setup (b), the distance between the two nozzles was about 4 mm
 141 forming a heating channel. The line of sight used in [17] was along the heating channel, i.e. in central
 142 position between the nozzles where turbulent gas flow in radial direction cannot be avoided and may
 143 disturb the observation of radial profiles. Having the opportunity to use quartz-sealed vertical slits,
 144 the observation point was positioned in one of the nozzles (the nozzle on the left side in Figure 2). It
 145 was at half distance to the electrode tip and the nozzle exhaust in the heating channel, i.e. about 9 mm
 146 away from both.

147 The arcs were operated under ambient conditions in case of setup (a), i.e. without external
 148 chambers. Setup (b) was part of a model circuit breaker that is shown in Figure 2. It was placed in an
 149 outer vessel of about 300 l volume that was evacuated and filled with CO₂ before each shot. Additional
 150 windows in the model chamber and the vessel allowed a free view through the nozzle. Thus, also in
 151 this case an observation was possible from opposite directions as well as absorption measurements.

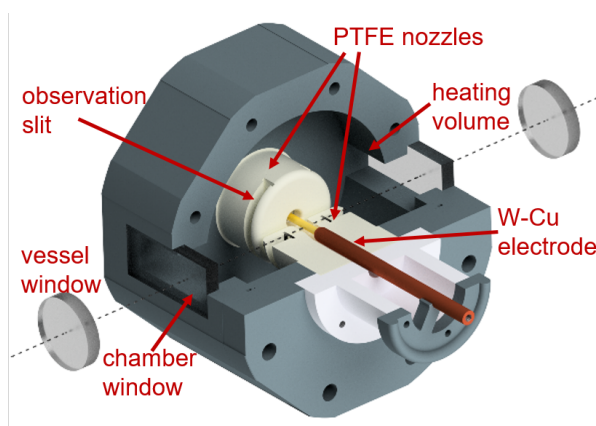


Figure 2. Setup (b) with the model circuit breaker inside a pressure vessel with vessel windows and the quartz plates in the observation slits. The dotted line indicates the sight through the outer vessel.

152 LC circuits were used to generate sine-like current waveforms of about 100 Hz frequency and
 153 11 kA peak current for setup (a) and 50 Hz and 5.3 kA for setup (b). The arc discharges were initiated
 154 using exploding thin Cu wires. Pressure sensors (603A from Kistler) were positioned in case of setup
 155 (a) in the middle of the nozzle, i.e. in 90° to the observation slits. In case of setup (b) the pressure
 156 sensor was placed in the heating volume of the model circuit breaker.

157 2.2. Optical setup

158 Different methods were applied for the optical analysis. Firstly, high-speed cameras (HSC), the
 159 24bits color Y6 or the 10bits monochrome Y4, both from Integrated Design Tools (IDT), were used
 160 to observe the general discharge behavior. Although the available area was reduced to a 2 mm-wide
 161 slit, relevant information was obtained regarding gas flow, asymmetry, dust, and droplets. As an
 162 example, a special double frame optics (DFO) could be applied between camera and lens that divided
 163 the optical path into two ways and produced two images of the same area that could be filtered at
 164 different wavelengths.

165 Secondly, optical emission spectroscopy was carried out by means of an imaging spectrograph
 166 with 0.5 m focal length (Roper Acton SpectraPro SP2500i). The nozzle slit was imaged on the
 167 entrance slit of the spectrograph by a focusing mirror to spectrally investigate arc cross sections,
 168 i.e. perpendicular to the arc axis. Having the development during arc discharge in the focus, the
 169 spectrograph was equipped with a high-speed video camera (Y4 series of IDT). That enabled to record
 170 series of 2D-spectra with typical repetition rates of 100 μ s, allowing about exposure times of 98 μ s
 171 (frame rate of 10 000 fps). It should be noted that rather long exposure times were necessary due to
 172 limited sensitivity of non-intensified HSC. Alternatively, the HSC was replaced by an ICCD camera
 173 (PI-MAX4 from Princeton Instruments) with higher sensitivity, allowing only single images but of
 174 shorter exposure times and at lower intensities, e.g. around current zero.

175 In a compromise between light intensity, spectral resolution, and exposure time, the entrance slit
 176 of the spectrograph was set to 50 μ m. With gratings of 150 lines per mm for overview and 1 800 l/mm
 177 for detailed spectra, the spectral range was 150 nm and 10 nm, and the spectral resolution (full width
 178 half maximum) 0.7 nm and <0.1 nm, respectively. The intensity of side-on spectra was calibrated in
 179 units of spectral radiance by means of a tungsten strip lamp (OSRAM Wi 17/G) at the arc position.
 180 The window transmission of 50–70 % was taken into account, mainly resulting from the coating of the
 181 quartz plates at the nozzles.

182 A positioning laser was used to adjust line of sight and check the stability between the shots.
 183 However, it was found that the width of 2 mm of the observation slit at the nozzle allowed a stable
 184 and free optical path. Usually, no corrections between the shots were needed thanks to the absence of
 185 moving parts.

186 3. Results

187 3.1. Video observation and flow reversal

188 On the left side of Figure 3, a typical current waveform (red) is shown for the discharges in the
 189 model circuit breaker with 5.3 kA peak value (setup (b)). The current has not exactly the shape of a
 190 perfect sine and a slightly longer duration than expected for 50 Hz (~ 10.6 ms). In this article the main
 191 focus is set on the time around CZ while the starting phase is of minor interest. Consequently, all
 192 points in time are given with respect to the current zero crossing for easier comparison. The voltage
 193 curve (blue) is characterized by a long period of values around 200 V flanked by two distinct peaks at
 194 explosion of the ignition wire and at the arc extinction near CZ. During the high-current phase of arc
 195 discharge, the voltage increases from the local minimum of about 140 V at the end of the ignition peak
 196 (10 ms) to a maximum of about 240 V during the peak current (5 ms), and slightly decreases again with
 197 lower currents until about 200 V (3 ms before CZ).

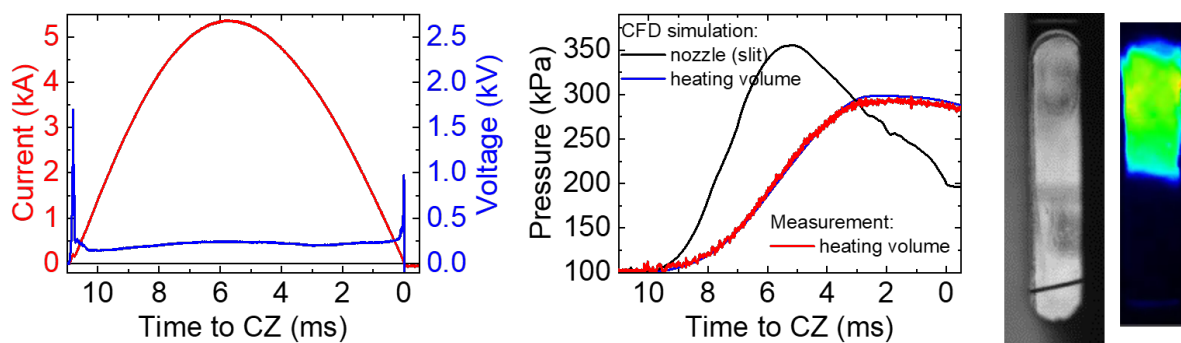


Figure 3. Left: Current and voltage waveform - nearly sine 50 Hz shape and duration (~ 10.6 ms). Middle: Pressure simulation for two positions and measurement for heating volume. Right: Photo (grey) of window with ignition wire and example for observation of the general behavior of the discharge about 1 ms before CZ (false color representation) showing asymmetric position of a constricted arc.

198 The intense radiation emitted from the arc plasma is absorbed by the surface of a surrounding
 199 PTFE nozzle where it causes photo-ablation of the wall material [13]. Part of the ablated material is
 200 exhausted as vapor by axial flow, the other part enters the arc and is heated to plasma temperature
 201 by absorption of radiation coming from the arc interior, leading to a discharge that is dominated by
 202 the ablation [18]. Both arc plasma and vapor create an overpressure which causes an axial expansion
 203 flow towards the ends of the nozzle. In the middle of Figure 3, three curves of the pressure are
 204 shown. The red and the black curve were obtained for the slit position inside the PTFE nozzle and
 205 the heating volume, respectively, from CFD simulation (CFD-ACE+ software suite by the ESI Group)
 206 of the discharge according to [17]. Comparison of simulation results for the heating volume (black)
 207 with our measurements (dashed blue) resulted in good agreement concerning the shape of the curve.
 208 Small deviations of the absolute values were used to adjust the pressure in the model. Although no
 209 pressure sensors could be placed directly in the nozzle or heating channel in case of the MCB, values
 210 of the pressure at OES position (slit) could be easily obtained from comparison with results from CFD
 211 simulation (red curve). The maximum pressure of 3.5 times the filling pressure is built up close to the
 212 peak current. It should be noted that at CZ the pressure is still about two times the filling pressure,
 213 which results in a cooling of the arc.

214 On the right part of Figure 3, a grey scale image is shown to illustrate the area of HSC observation
 215 at the position of the nozzle slit. Note that illumination from backside was applied; the ignition wire
 216 can be recognized in the lower part. Finally, an example of a HSC frame of the arc in false colors
 217 is given on the far right about 1 ms before CZ. Typically, the arc is constricted at this time to less than

218 half of the nozzle diameter. Here, it is located in the upper part of the nozzle, showing deviation from
 219 rotational symmetry.

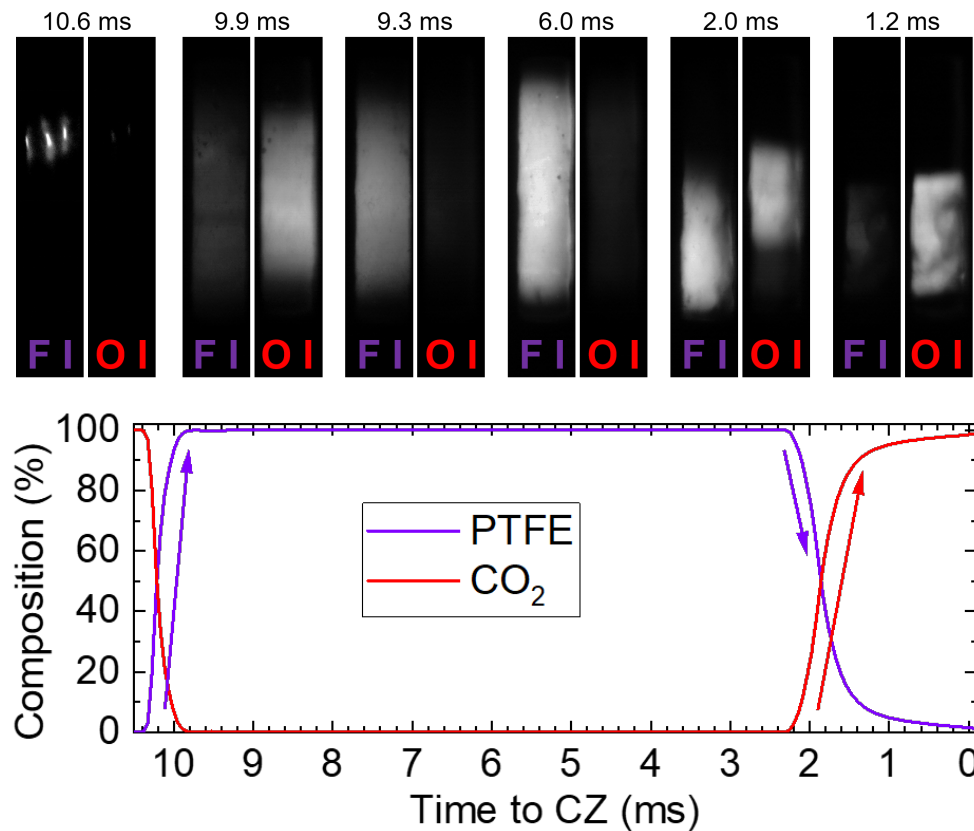


Figure 4. Visualization of the flow reversal before CZ for setup (b). Top: Selected frames of HSC imaging using double frame optics; filters were applied for the atomic line emissions of F I 675 nm (left channel) and of O I 777 nm (right channel) to visualize emission from PTFE and CO₂, respectively. Bottom: Plasma composition as obtained from CFD simulation.

220 The arc in the slit area was further investigated using the double frame optics (DFO). Filters were
 221 applied to reveal information on the plasma composition. Any emission from fluorine and oxygen
 222 can be clearly dedicated to the nozzle wall (PTFE, C₂F₄) and filling gas (CO₂), respectively. Therefore,
 223 the left channel was equipped with a metal interference filter (MIF) with maximum transmission at
 224 675 nm to become sensitive for several atomic fluorine lines F I and the right channel with a narrow
 225 filter at 777 nm for the atomic oxygen triplet O I. The emission from carbon lines could not be used
 226 since both materials contained carbon. On the upper part of Figure 4, six exemplary double frames are
 227 shown for significant points in time. In the lower part of Figure 4 the plasma composition as obtained
 228 from the CFD simulation is shown as fractions of PTFE and CO₂.

229 The first frame from the DFO mainly shows the atomic copper emission from ignition wire that is
 230 present on the left side (Cu I line at 674.1 nm). The wire was divided by explosion into three pieces
 231 within the 2 mm slit area. Less than a millisecond later, the emission dominated in the right channel,
 232 indicating a discharge in the CO₂ atmosphere (9.9 ms to CZ). Within few hundreds of microseconds,
 233 the brightness of the right channel faded while the left part became more intense. Here, the increasing
 234 wall ablation started to dominate the discharge, blowing the fill gas out of the nozzle. This is in
 235 good agreement with the simulation results. In the following, a long and stable period was observed
 236 that was dominated by ablation (cf. frame at 6.0 ms before CZ). Another reversal of flow was found
 237 about 2 ms before CZ: When the arc current and thus wall ablation were considerably decreased, the
 238 pressure in the nozzle also decreased to values below that of the heating volume, cf. Figure 3. As

239 a consequence (relatively cold) gas from the heating volume with high fraction of CO₂ flowed back
 240 into the nozzle. There it was heated up by the arc current, and its radiation could be seen in the right
 241 channel. Interestingly, different intensity distributions were found for left and right channel at 2.0 ms
 242 before CZ. That indicated non-homogeneous gas mixture. Finally, only emission from O I could be
 243 seen in the last ms, indicating a plasma composition completely dominated by CO₂.

244 3.2. OES of high-current phase using high-speed camera

245 Series of two-dimensional spectra were obtained by means of video spectroscopy, allowing to
 246 investigate the different phases of the discharge within one acquisition (setup (b) with same conditions
 247 as above). This is illustrated in Figure 5 where six selected frames of one shot are shown exemplarily.
 248 The vertical dimension of each frame is related to the spatial distribution of the arc cross section along
 249 the nozzle slit whereas the spectral distribution is represented by the horizontal dimension. The
 250 major lines and the time in relation to current zero are labeled above and on the left, respectively. For
 251 line classification, energy levels, transition probabilities, and other information on spectral lines the
 252 databases from NIST [21] and Kurucz [22] were applied. The spectra are dominated by line emission
 253 of Cu, C, O, and F with highest intensities in the central part of the axis. Those lines could be utilized
 254 for an analysis of temperature profiles along most of the arc radius. In cases with significant nozzle
 255 ablation, usually F I or C II lines were applied [11,12,17].

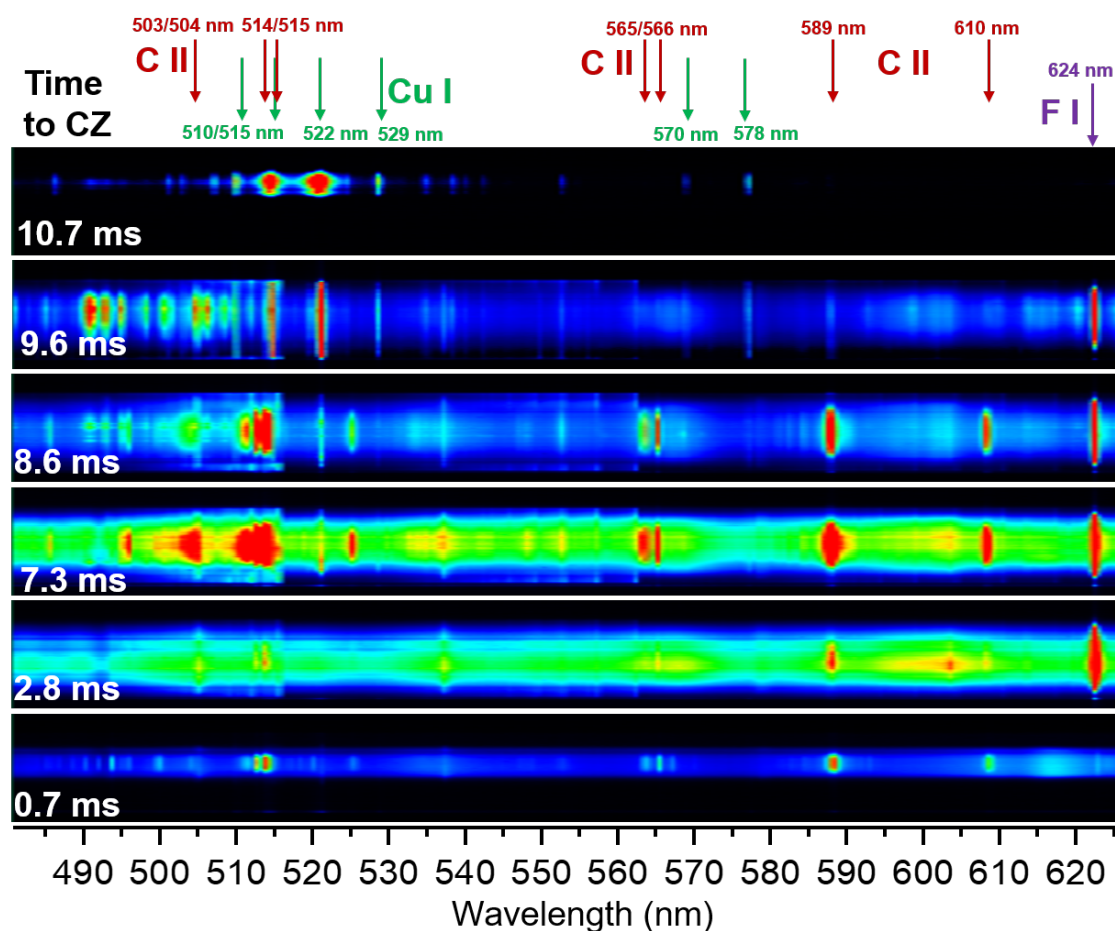


Figure 5. 2D-OES frames acquired at selected time points during one discharge by video spectroscopy with setup (b). From top to bottom: Ignition phase dominated by atomic Cu I lines from wire, transition to ablation-dominated arc with ionic C II and atomic F I lines from PTFE and close to CZ only C II from CO₂.

256 The first spectrum with detectable light emission acquired during the initial phase (10.7 ms before
257 CZ) is characterized by the exploding ignition wire made of copper. Thus, only atomic Cu I lines
258 are visible (labeled by green arrows). Obviously, the wire position was slightly off-axis for this shot.
259 Although an influence of the ignition wire can be proved to last up to 1 ms, the bright peak is much
260 shorter, typically below 100 μs [16]. Next, the filling gas CO_2 causes an additional emission of carbon
261 ionic C II lines (red) and of the oxygen lines (O I at 777 nm, not shown here). This emission was found
262 to be visible in OES after 100-220 μs . Under extreme conditions, i.e. for the setup (a) with the tubular
263 PTFE nozzle exposed to high peak currents of 11 kA at 100 Hz, the lines of Cu I, C II and O I can
264 have intensity peaks already 300-400 μs after ignition, while the F I emission (from PTFE) starts about
265 300-400 μs after ignition [16].

266 Further emission of Cu I lines can be observed due to erosion of the W-Cu electrode, cf. the
267 second spectrum at 9.6 ms before CZ. Here, the Cu I emission is still intense and distributed over
268 the whole nozzle diameter. Additionally, rather weak carbon ionic as well as much brighter atomic
269 fluorine lines (F I at 624 nm only in this spectral range) are visible. Although the influence of CO_2 is
270 strongly decreased at 9.6 ms to CZ as it is known from the DFO investigation and plasma composition
271 calculation, a ratio in particle density of about 1:2 of carbon to fluorine can be expected (C_2F_4 are the
272 building blocks of PTFE). The transition probabilities of the line emission are roughly comparable, e.g.
273 summarizing to about $10 \times 10^7 \text{ s}^{-1}$ for three C II lines at 609/610 nm and about $3 \times 10^7 \text{ s}^{-1}$ for the F I
274 line at 624.0 nm. Considering the much stronger F I emission this means that excitation of F I with
275 upper level at $\sim 14 \text{ eV}$ is much more pronounced than an ionization of carbon atoms and excitation of
276 C II with $\sim 24 \text{ eV}$.

277 The third spectrum at 8.6 ms before CZ is acquired in the phase of increasing PTFE nozzle ablation
278 that causes stronger emission of both atomic fluorine and carbon ionic lines. Furthermore, the C II and
279 F I lines have comparable intensities, indicating more ionization and excitation of the C II levels than
280 before and thus, considerable higher temperatures of the arc. The vanishing Cu I indicates that the
281 metal vapor from electrode erosion is blown "backwards" by the new established flow of hot, ablated
282 nozzle material.

283 Approaching peak current (7.3 ms before CZ), also continuum radiation can be observed. On the
284 one hand, there is a very broad continuum over the whole spectral range that is mainly emitting in
285 the center of the arc. On the other hand, there is a pattern of many lines (often not resolved with this
286 spectral resolution) of increasing intensities with increasing wavelengths until rather sharp edges, e.g.
287 at 516 and 563 nm. This structure could be attributed to an emission of diatomic carbon molecules, i.e.
288 the Swan band system arising from transitions between the $d^3 \Pi_g$ and the $a^3 \Pi_u$ electronic states of
289 C_2 molecules. These Swan bands will be discussed later in detail. It should be noted that its spatial
290 distribution ranges over the whole nozzle diameter, partially with peaks near to the nozzle walls.

291 With decreasing currents, the intensity of ionic C II lines decreases again; the atomic F I line at
292 624 nm has a much higher intensity at 2.8 ms before CZ whereas the C II lines are much weaker. Similar
293 to the third spectrum at 8.6 ms to CZ, the excitation of ionic states is much less pronounced than that
294 of fluorine atoms with upper levels around 14 eV due to significantly lowered plasma temperature.

295 In the following phase of low current, the radiation emitted by the arc plasma does not longer
296 cause sufficient wall ablation to sustain the high pressure in the nozzle (cf. spectrum at 0.7 ms before
297 CZ). The consequences are reversal of the gas flow direction, disappearance of the fluorine line, and a
298 spectrum dominated by C II line emission originating from the back-flowing CO_2 from the heating
299 channel (plus continuum). Furthermore it should be noted that the arc is constricted, i.e. only a rather
300 small part of the radial profile carries contribution to emission and thus, also to electrical conductance.

301 3.3. Optical emission spectroscopy near to current zero

302 In the following the phase around current zero will be investigated for both nozzle geometries.
303 Besides, the potential and limits of optical emission spectroscopy shall be discussed. The long, tubular
304 nozzle of setup (a) is used to produce intense and short discharges (11 kA at 100 Hz) that will be

305 analyzed by OES with high-speed camera (HSC). Investigations with the more realistic setup (b) in
 306 the model circuit chamber (5 kA at 50 Hz) will be carried out using OES with intensified CCD (ICCD)
 307 camera to come as close as possible to CZ.

308 3.3.1. OES with high-speed camera

309 At first, the case of a current zero phase after an intense arc is considered. A strong PTFE wall
 310 ablation and pressure built-up is realized with the higher current of 11 kA peak. Using setup (a), the
 311 material flow is directed towards the exhausts at both electrode sides since the tubular nozzle is not
 312 interrupted, e.g. by a heating channel. Thus, the plasma is expected to remain relatively hot and dense
 313 for longer time near CZ, at least in the observation position in the middle of the tube. It should be
 314 noted that the setup does not perform switching, i.e. the current is continued after CZ with reversed
 315 polarity. Additionally, there is only a short period of low current, i.e. it takes only ~ 2.5 ms from peak
 316 to CZ for 100 Hz. With other words, best conditions are chosen for analysis of the fluorine lines close
 317 to CZ.

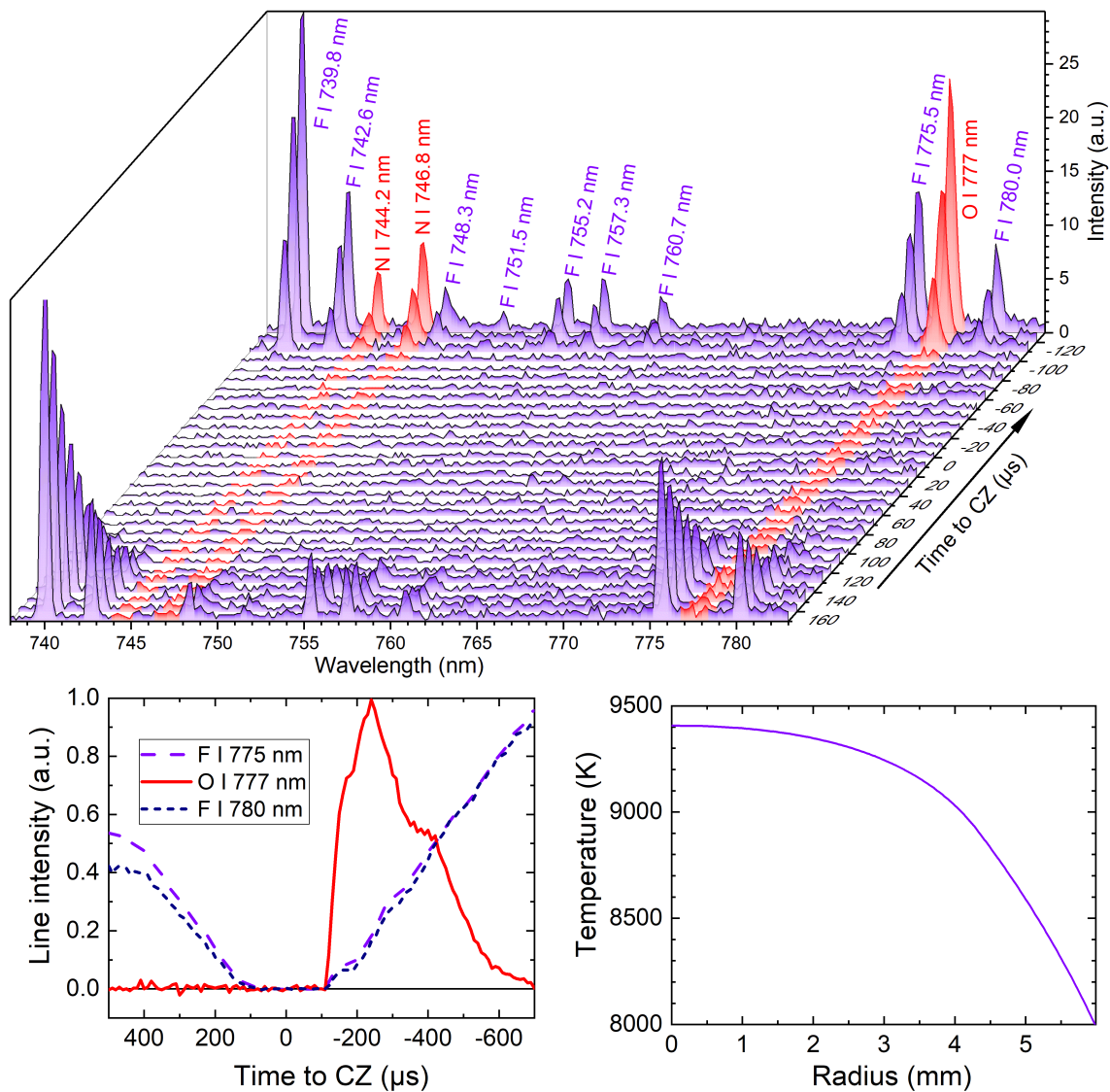


Figure 6. Top: Temporal evolution of spectra around current zero in the arc center for setup (b). Note the direction of the timescale from bottom to top. Bottom left: Temporal evolution of three selected line intensities. Bottom right: Radial temperature profile acquired 400 μ s before CZ.

318 Concerning imaging spectroscopy with high-speed camera, both temporal and spatial resolution
319 are of interest. However, a limit was given by the detector's readout rate. Hence, highest temporal
320 resolution was obtained by drastic reduction of the number of vertical lines, practically giving up the
321 spatial dimension (side-on information). In the following, only the central position is used to analyze
322 the temporal evolution of the spectrum with a frame rate of 100 kfps (10 μ s repetition rate). In the
323 upper part of Figure 6, the spectral evolution around CZ is shown. It should be mentioned that neither
324 the full spectral range nor all spectra acquired during the discharge are plotted in order to focus on
325 distinguishable lines of the relevant species during the phase around current zero. Some major lines of
326 atomic fluorine as well as oxygen and nitrogen are labeled. Although there were no lines from carbon
327 observed in the diagrammed spectral range (738-783 nm), other lines were checked and confirmed the
328 finding described below, e.g. the ionic carbon lines C II 658 nm and 723 nm.

329 Among the 30 successive spectra shown in Figure 6, 17 were taken before and 13 were taken
330 after CZ (see timescale at Y-axis and arrow). As expected for an ablation-dominated arc, only the
331 F I lines were found, cf. spectra from 170 μ s to about 100 μ s. The line intensities rapidly faded out
332 due to low decreasing energy input by the arc. Then a "dark" phase followed without detectable
333 emission starting from about 100 μ s before and lasting until about 100 μ s after current zero. During
334 this dark phase, other spectral techniques would be necessary for investigation of the residual plasma,
335 e.g. intensified cameras for emission spectroscopy or absorption measurements. The first spectra with
336 sufficient intensity after CZ shows a different behavior: Additional lines could be observed, namely
337 the oxygen triplet O I at 777 nm and three N I nitrogen lines around 744 nm. They are marked by red
338 color to differ them from the fluorine lines and to prove that they were not detectable before CZ. This
339 demonstrates the back-flow of ambient air containing oxygen and nitrogen into the nozzle after CZ.
340 The temporal evolution of three exemplary lines is shown in the left lower part of Figure 6. It should
341 be mentioned that for this plot first the line integral of each of the three lines was calculated, second
342 the intensity at line edges (lower / higher wavelength) was taken as "line background signal" and
343 subtracted, and finally the intensities of these line integrals were normalized for better comparison.
344 The two fluorine lines show very similar behavior, decreasing before and increasing intensity after CZ
345 with comparable falling / rise rates. In contrast, the oxygen lines (triplet 777 nm) have an intensity
346 of background level during all times before and until 100 μ s after CZ. Then they rise up very fast, i.e.
347 from zero to a maximum level within about 100 μ s. A slower decrease follows; however, they can be
348 detected until 500-600 μ s. Thus, for both the ignition phase as well as the current zero crossing, it can
349 be stated for the high current and setup (a) that the arc plasma needs about 0.5-1.0 ms to be completely
350 dominated by the ablated wall material and the influence of the surrounding gas can be neglected - at
351 least under ambient conditions of one bar air.

352 The next step is the determination of radial temperature profiles as close as possible to current
353 zero with HSC. Hence, sufficient spatial resolution is required. Therefore, the number of lines used for
354 the two-dimensional spectra was increased to 600. As a consequence, the repetition rate and thus, the
355 temporal resolution had to be reduced to 133 μ s and 7500 fps, respectively. Hence, the dark phase is
356 reduced to one spectrum only. Furthermore, there are two spectra directly before CZ with an emission
357 sufficient for F I line detection but not for plasma temperature determination due to restrictions in
358 the signal-to-noise ratio. The third spectrum, i.e. 400 μ s before CZ, could be applied. An absolute
359 intensity calibration of the 2D-spectrum was done by means of a tungsten ribbon lamp. Then Abel
360 inversion was carried out to obtain radially resolved emission coefficients under the assumptions of
361 an optically thin plasma and rotational symmetry of the arc. Finally, radial temperature profiles were
362 determined assuming a plasma composition of 100% C₂F₄ at atmospheric pressure (no contribution
363 from electrodes or air) and local thermodynamic equilibrium. Several fluorine lines were applied for
364 comparison, yielding similar results. The temperature profile shown in the right part of Figure 6 has a
365 maximum of 9400 K in the arc center and is rather broad: Even at a radial position of about 4 mm, i.e.
366 2 mm away from the nozzle wall, the temperature is still around 9000 K. In close vicinity to the wall, it
367 decreases rapidly to values around 8000 K.

368 3.3.2. OES with intensified camera

369 At second, the case of a current zero phase shall be investigated under the more realistic setup (b)
 370 in the model circuit chamber filled with 1 bar CO₂ (5 kA at 50 Hz). The high-speed camera is replaced
 371 by an ICCD camera. Thus, an improvement in sensitivity can be demonstrated as a side-effect. An
 372 example of a two-dimensional spectrum is shown in the upper part of Figure 7. It was acquired 300 μs
 373 before CZ with an exposure time of 200 ns. The vertical axis comprises the full nozzle cross section
 374 with a diameter of 12 mm.

375 Obviously, the arc was contracted to few mm due to the low current (<500 A) and was slightly
 376 shifted upwards, i.e. not in the center of the nozzle. For further analysis, the symmetry axis had to be
 377 shifted by about 1.5 mm from the nozzle center to the central position of the arc. Thus, symmetrization
 378 of the two sides ("upper" and "lower") can be carried out, providing a side-on spectrum with spatial
 379 dependence from central to outer side-on positions. The spectral radiance for the position of the arc
 380 center is given as an 1D-spectrum in the middle of Figure 7. Because of the CO₂ gas filling, atomic
 381 oxygen (O I 715 nm, 777 nm) and ionic carbon (C II 658 nm, 723 nm) lines are found, but none from
 382 fluorine, e.g. F I at 775.5 nm, 780.0 nm. In general, F I can be detected definitely at 2 ms but never
 383 1 ms or less before CZ under these conditions, cf. the collection of spectra at different times before

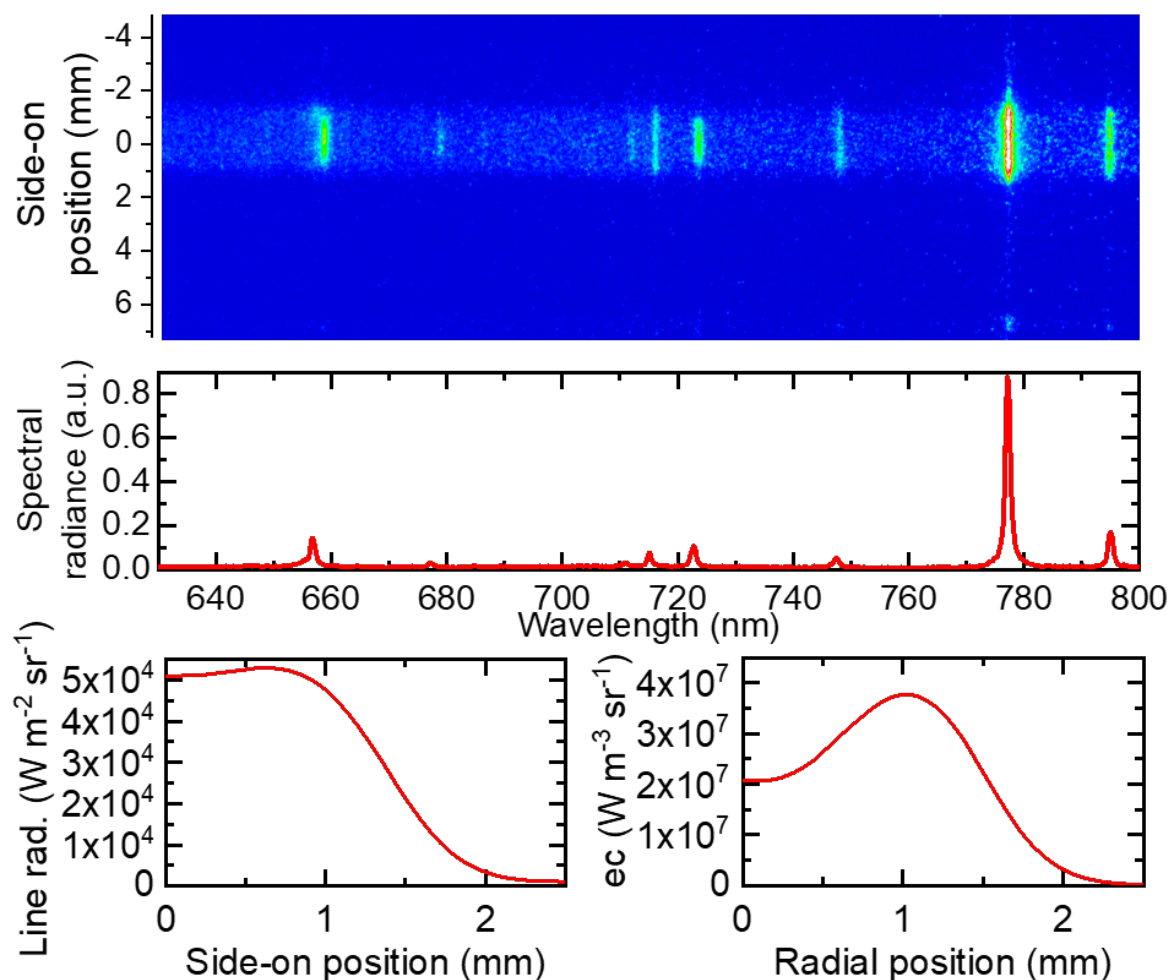


Figure 7. Two-dimensional spectrum measured 300 μs before CZ by ICCD camera to gain higher sensitivity in comparison to HSC (top). Vertical axis comprises the nozzle diameter of 12 mm. After shifting the axis to the central position of the arc and symmetrization, side-on radiance was obtained by integration over the O I 777 nm triplet (bottom left). The deduced emission coefficient (bottom right) shows a distinct maximum at 1 mm caused by the higher ionization degree in the arc center.

384 CZ shown below in Figure 10. This is a consequence of the different setup and the lower arc current
 385 compared with the case described above (lower peak current of 5 kA instead of 11 kA, and longer
 386 duration of the half-wave of 10.7 ms instead of 5 ms), yielding less vapor from PTFE ablation.

387 Both the ionic carbon and the atomic oxygen lines were used for analysis of the radial temperature
 388 distribution. In the following, the procedure will be described for the oxygen triplet. At first step, an
 389 absolute intensity calibration was carried out. Secondly, the total radiation flux of the O I 777 nm triplet
 390 was obtained by spectral integration over the line ($\sim 775\text{--}780$ nm with correction using left and right
 391 background) for each side-on position; the resulting line radiance in units of $\text{W m}^{-2} \text{sr}^{-1}$ is plotted
 392 in the left bottom of Figure 7). This side-on profile was found to be rather flat in the first millimeter
 393 beginning from central position and to decrease practically to zero within another millimeter. Although
 394 the arc center was not in the nozzle center, it could be assumed that the main path of current flow
 395 has sufficient rotational symmetry for the application of an inverse Abel transformation. Hence, in
 396 the third step the radial-dependent emission coefficient ec of the O I triplet could be determined as
 397 shown in the right bottom of Figure 7. A distinct maximum of ec was found at a radial position of
 398 $R_{max} \approx 1$ mm; towards the arc center ec decreased again though higher temperatures are to be expected
 399 there. Such a behavior gives hint that the "normal maximum" of the emission coefficient for a line
 400 transition is reached. This maximum results from ionization which decreases the available number of
 401 atoms to be in an excited level with increasing temperature. For better illustration, the temperature
 402 dependence of the emission coefficient is plotted in the left part of Figure 8. It was calculated on base of
 403 NIST data for different pressures of pure CO_2 assuming optically thin plasma. The normal maximum
 404 was found to be around 16 000 K with only weak dependence on the pressure, cf. right part of Figure 8.
 405 It should be noted that the maximum emission coefficient has nearly linear dependence on the CO_2
 406 pressure since it principally reflects the density of the radiating species.

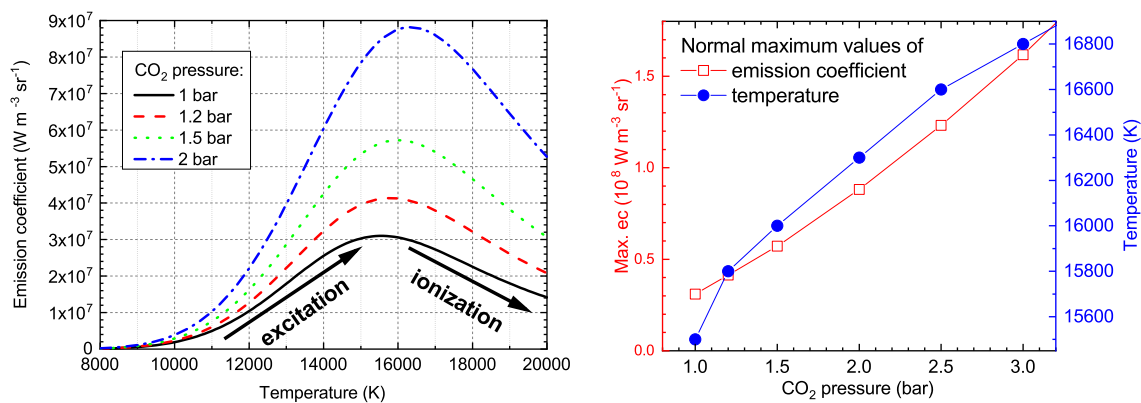


Figure 8. Left: Calculated emission coefficient of the O I 777 nm triplet at different partial pressures of CO_2 depending on temperature. Note that the normal maximum is strongly dependent on the pressure but its position is rather stable around 16 000 K. Right: Pressure dependence of emission coefficient and temperature at normal maximum.

407 As fourth step to temperature profiles, plasma temperatures can be obtained from the
 408 experimentally determined emission coefficients by comparison with the calculated values in Figure 8.
 409 Therefore, in the case of experimental ec from the "outer" part of the arc, i.e. values for radial
 410 position $r > R_{max}$, the left wing of the curve ("rising" = temperatures below normal maximum)
 411 has to be applied, while for the arc center $r < R_{max}$ the right wing is valid ("falling" = temperature
 412 above normal maximum). Knowing the pressure and plasma composition, an absolute value of the
 413 emission coefficient would not be mandatory. Hence, the absolute intensity calibration gives additional
 414 information and allows to validate the experimental methods and assumptions. In general, the highest
 415 experimentally determined emission coefficients fitted best to the calculated normal maxima for a
 416 plasma composition of pure CO_2 with 1.2 bar total pressure. The ionic carbon line C II at 658 nm shows
 417 the normal maximum at around 22 000 K. The experimentally obtained ec did show no indication for

418 temperature above the normal maximum - which proves that double ionization was rather improbable
 419 in accordance with earlier studies. Hence, for C II only the left wing with "rising" *ec* were applied.
 420 However, the experimentally obtained emission coefficients are higher than the normal maximum
 421 calculated for a pressure of 1.2 bar in pure CO₂ (the assumption used for the evaluation of the O I
 422 triplet). This is an indication that an additional amount of carbon is in the gas mixture eventually
 423 originating from the delayed evaporation of carbon soot particles produced during nozzle ablation.
 424 Because the gas composition and pressure could not be determined accurately, pure CO₂ but with an
 425 enhanced pressure of 2 bar (close to the results of CFD simulations) was assumed for the evaluation of
 426 the *ec* of the C II line.

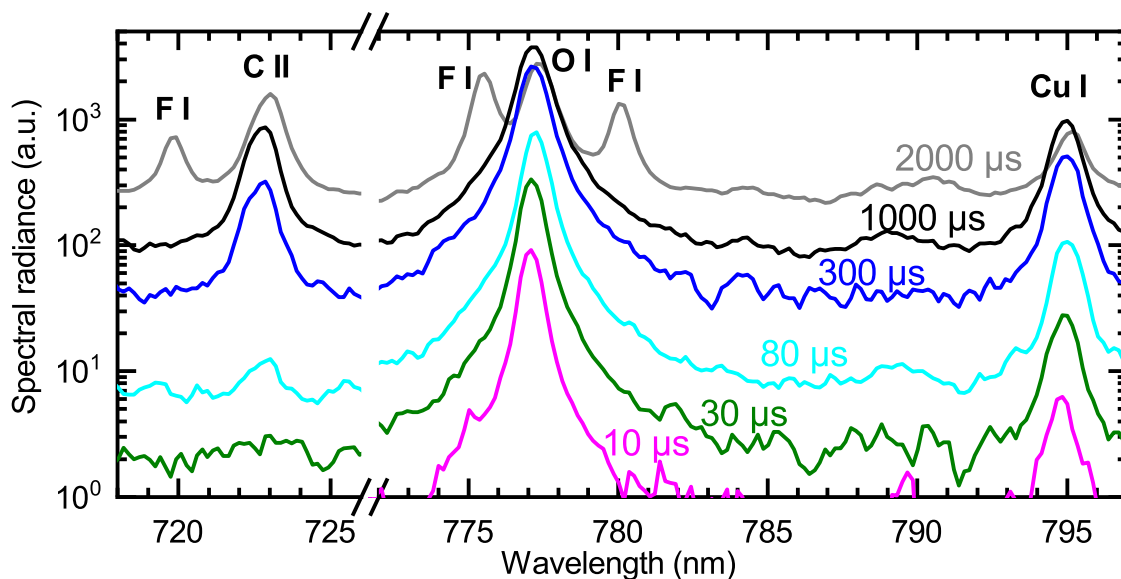


Figure 9. Selection of spectra acquired at different instants of time before current zero.

427 Spectral radiances for different instants of time before current zero are shown in Figure 9. For a
 428 better visibility, only parts of the spectral range comprising the most relevant lines and six selected
 429 spectra are plotted. A logarithmic intensity scale is used to show the enormous decrease of line
 430 intensities, e.g. by about 2 orders of magnitude for O I and Cu I. Note that the exposure time had to be
 431 increased from 0.2-0.5 μ s to 2.0 μ s for all spectra closer to CZ than 150 μ s due to decrease of intensity.
 432 Fluorine atomic lines were found only in the gray spectrum acquired 2 ms before CZ, proving that
 433 under the conditions of this setup and current waveform the influence of ablated wall material was
 434 negligible \leq 1 ms before CZ. Carbon ionic lines could be detected until 80 μ s before CZ whereas atomic
 435 oxygen and copper lines were visible in all spectra.

436 The radial temperature profiles for five shots obtained from the emission coefficient of the C II at
 437 658 nm considering 100% CO₂ gas at 2 bar are plotted in the upper part of Figure 10. Only times of
 438 1 ms or less before CZ were taken into the analysis, i.e. the spectrum at 2 ms was excluded due to the F
 439 I lines indicating still PTFE admixtures. The spectrum acquired 1 ms before current zero resulted in
 440 a broad and flat temperature profile. The temperature between the arc center and 1.5 mm was more
 441 or less constant around 18 000 K. Then it was continued with a slow decrease to about 12 000 K at a
 442 radial position of nearly 4 mm, e.g. 2 mm away from the nozzle wall. This is a typical behavior of a
 443 wall-stabilized arc at moderate current. For the following spectra, i.e. taken after 400 and 300 μ s before
 444 CZ, two effects could be observed: (i) a considerable decrease of the arc diameter by nearly a factor of
 445 two that was accompanied by (ii) an increase of the core temperature to values above 20 000 K. Hence,
 446 a transition from the broad profile due to wall-stabilization to smaller, constricted profiles occurred.
 447 Since the arc current decreased not as fast as the square of the arc diameter, the core temperature
 448 had to be increased to provide a sufficient current density. In the following period, i.e. for times
 449 130-150 μ s before CZ, a further decrease of the arc diameter was found; however, the maximum plasma

450 temperature in the arc core could also be decreased due to further current decrease. Spectra acquired
 451 at less than $100 \mu\text{s}$ before CZ had too low intensities of the C II ionic line to allow for determination of
 452 reliable temperature profiles.

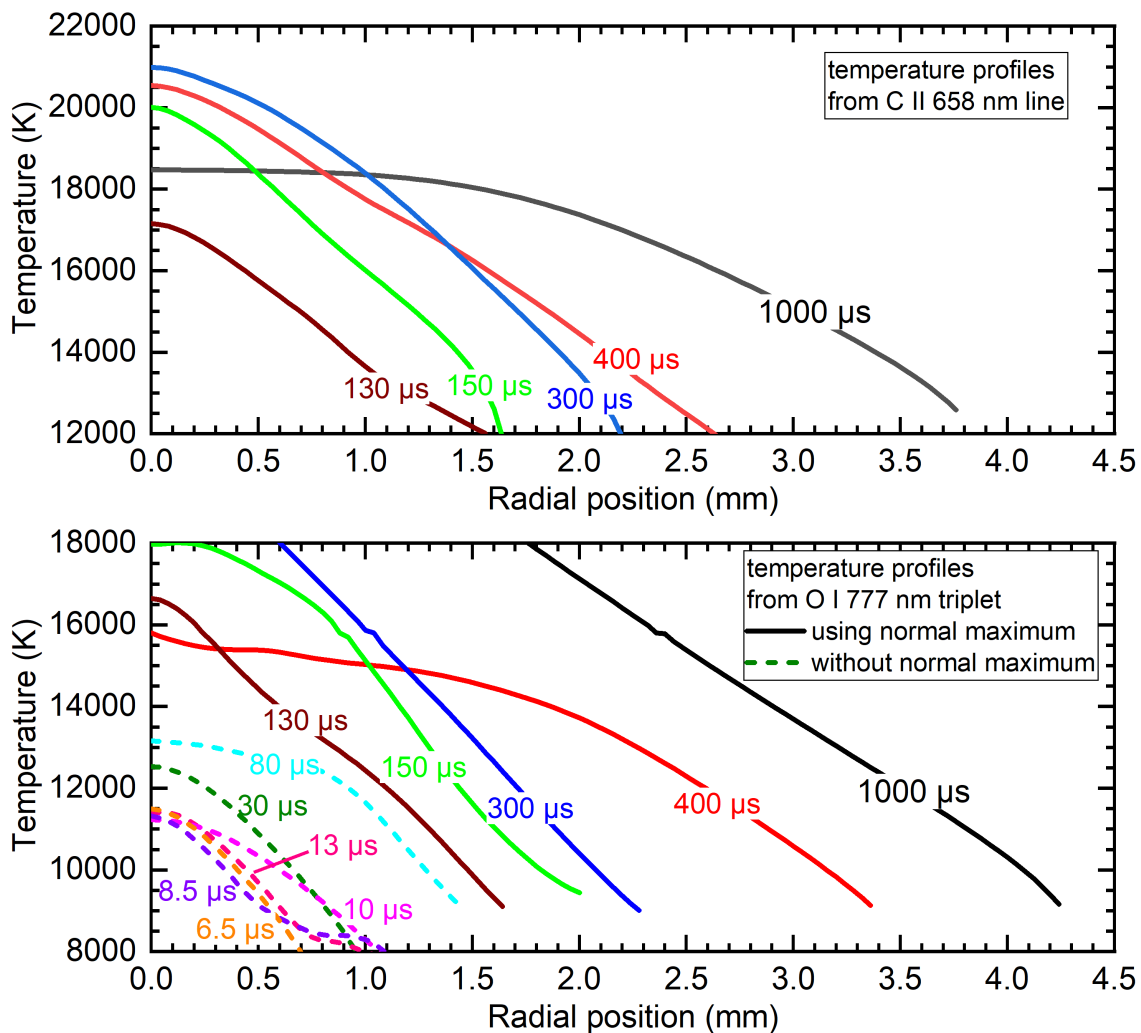


Figure 10. Radial profiles of plasma temperature obtained from ionic carbon line C II at 658 nm (top) and from atomic oxygen triplet at 777 nm (bottom) with (130–1000 μs) and without (<100 μs before CZ, dashed curves) application of normal maximum.

453 In the lower part of Figure 10, radial temperature profiles for numerous shots obtained from
 454 the O I triplet at 777 nm are plotted. Here, an emission coefficient for 100% CO_2 with 1.2 bar total
 455 pressure has been considered for the temperature determination. In agreement with the results for
 456 the C II line, the broadest profile with highest temperatures was obtained for 1 ms. Here, the position
 457 of the normal maximum connected with a fairly established temperature of 16 000 K was obtained at
 458 about 2.5 mm. Although the maximum temperature exceeded 20 000 K only values till 18 000 K were
 459 plotted due to higher uncertainties for the central position. However, the plasma temperature was still
 460 about 10 000 K even at a radial position of 4 mm, i.e. the arc was spread over most of the nozzle area
 461 (12 mm diameter). For the following profiles, the effect of temperature increase in the core was not as
 462 clear as above for C II. Though some profiles do not perfectly fit into the generally smooth decreasing
 463 behavior, the general tendency was that both arc diameter and maximum temperature in the center
 464 decrease continuously with decreasing current. The above described method based on the normal
 465 maximum of the oxygen triplet could be applied to all spectra taken ~ 100 – $1000 \mu\text{s}$ before CZ. For the
 466 remaining spectra (<100 μs) the experimental emission coefficients were below the normal maximum.

467 Hence, the common single-line method was applied using only the left ("rising") wing of the curve
468 from Figure 8. These temperature profiles are plotted as dashed curves in Figure 10. The tendency to
469 smaller profiles with lower peak temperatures can be followed until about 10 μs before current zero,
470 i.e. at very low currents of few tens of amperes. Although spectra (of 2 μs exposure time) were taken at
471 varying times of 13, 10, 8.5, and 6.5 μs before CZ and the exact acquisition times were measured by
472 comparison of current waveform and a monitor signal from the ICCD camera, nearly the same results
473 were obtained for all four shots: a temperature maximum slightly above 11 000 K and a decrease to
474 8 000 K within ≤ 1.0 mm. Here, the experimental limit is reached; possible changes in temperature
475 profile are superimposed by shot-to-shot variation of the discharge itself, window transmission and
476 uncertainties in determination of emission coefficient. As a control, another spectrum was acquired at
477 current zero (from 1.0 μs before CZ to 1.0 μs after CZ); however, only noise was recorded.

478 4. Discussion

479 4.1. General

480 An ablation-dominated arc of 5 kA peak current was operated in a model circuit breaker with CO₂
481 atmosphere. Application of a slit over the full radius of the PTFE nozzle enabled direct investigation
482 inside the nozzle. This was a substantial progress in comparison with previous measurements that
483 potentially suffered from an influence of turbulent gas flow in the heating channel [17]. Sealing by
484 thin quartz plates was proved to be an useful method to obtain reproducible conditions of discharges
485 without significant changes of material flow or plasma conditions. Consequent exchange of the plates
486 after each shot yielded to high window transmission with moderate blackening. An averaged overall
487 transmission of about 50 % was estimated along the observation axis made of the quartz plate in the
488 nozzle and the windows of the MCB chamber as well as the high-pressure vessel. The shot-to-shot
489 variation was usually about 10 %. Nozzle ablation caused widening of the nozzle diameter and thus a
490 slow reduction of maximum pressures over many shots. Therefore, the PTFE nozzles were exchanged
491 regularly. Only very few cases of reduced sealing quality occurred, easily noticeable after discharges
492 due to increased blackening at the plate's corners. These shots had to be repeated with renewed sealing.

493 The assets of different methods for optical investigation were demonstrated. Using high-speed
494 cameras the general arc behavior was investigated, e.g. revealing rotational symmetry over the
495 whole nozzle diameter in the high-current phase but not close to current zero when the stabilization
496 by ablation of nozzle wall was lost and the arc was constricted and out of the nozzle center.
497 Besides, the HSC allowed investigation of many successive points of time within the same shot.
498 Thus, reproducibility was not demanded and dynamic changes, their rising and falling times, and
499 shot-to-shot variation could be easily investigated. Although parameter variation was not in the
500 focus of this work, such investigations are rather comfortable using this technique. Furthermore, a
501 combination of HSC with double frame optics was introduced; filtering one channel only for radiation
502 from CO₂ (O I at 777 nm) and the other channel only for emission from PTFE (F I at 675 nm) allowed
503 to gain knowledge about the temporal evolution of the plasma composition. In combination with
504 according CFD simulation, gas flow behavior could be analyzed, including the exact determination of
505 the point in time when flow reversal occurred before current zero. In the experiments described here,
506 only qualitative analysis could be carried out. For a quantitative description, more knowledge about
507 plasma composition and absolute intensity calibration would be mandatory [23].

508 4.2. OES using HSC

509 Deeper information was obtained from spatially and temporally resolved video spectroscopy
510 using HSC. That comprised the different phases of discharge and the occurrence of Swan band emission
511 from C₂ molecules that are treated in an accompanying publication [20]. Radial temperature profiles
512 have been determined until 400 μs before current zero. Assuming a plasma composition of 100 % C₂F₄
513 at atmospheric pressure, a broad temperature profile has been obtained with a maximum of 9400 K in

514 the arc center and about 9000 K at a radial position of about 4 mm, i.e. 2 mm away from the nozzle wall.
515 Several fluorine lines were applied for comparison, yielding similar results. A "dark window" without
516 detectable emission was observed due to low intensities caused by cold gas flow and low current on
517 the one hand and limitations in the sensitivity of high-speed cameras on the other hand, starting in
518 best case about 100 μs before CZ. Furthermore, it could be stated for the high current and setup (a) that
519 the arc plasma needs about 0.5-1.0 ms for both the ignition phase as well as the current zero crossing to
520 be completely dominated by the ablated wall material. The influence of the surrounding gas can be
521 neglected - at least under ambient conditions of one bar air.

522 4.3. OES with ICCD

523 The sensitivity of OES was increased by application of OES with an intensified CCD camera,
524 allowing single-shot measurements until few μs before current zero. Two lines were used for
525 determination of temperature profiles of the arc plasma: Whereas the ionic carbon line C II at 658 nm has
526 a normal maximum around 22 000 K and therefore better sensitivity concerning temperatures around
527 18 000-20 000 K, the atomic oxygen triplet O I at 777 nm has its normal maximum around 16 000 K and
528 higher sensitivity at lower temperatures. Off-axis maxima of the radial emission coefficient of the
529 O I triplet were found indicating temperatures in the arc center above and in the arc fringes below
530 the normal maximum. Hence, the normal maximum can be used for the calibration of the emission
531 coefficient according to the Fowler-Milne method. In addition, the absolute intensity calibration by a
532 radiation normal has been used for verification. The emission coefficient of the C II line was evaluated
533 with absolute intensity calibration only.

534 As experimental uncertainties of the determined emission coefficients, in particular the window
535 transmission (estimated to $50\% \pm 10\%$), adjustment of slit width ($50 \pm 5 \mu\text{m}$), performing of absolute
536 intensity calibration (uncertainty up to 20%), and pressure measurement (uncertainty up to 10%) have
537 to be considered. It is an advantage of the applied method for the O I triplet that the normal maximum is
538 independent from influences by transmission, absorption, and absolute intensity calibration. Therefore,
539 the uncertainty of the temperature determined from O I is low around the normal maximum of
540 16 000 K as well as in the range of 10 000–14 000 K (up to 10%) due to exponential intensity rise with
541 temperature. However, reliable temperatures above 20 000 K cannot be determined from the O I triplet.
542 An important factor is the remaining uncertainty of the gas composition and the partial pressure
543 of carbon and oxygen. Pressure measurements showed a shot-to-shot variation between 0.2 and
544 0.4 bar, and the fitting of the emission coefficients of the C II line and the O I triplet with respect to
545 the corresponding normal maximum in pure CO_2 lead to the different pressures 1.2 and 2 bar. But
546 considering the relatively low variation of the temperatures at the normal maxima with pressure, the
547 uncertainty of the plasma temperatures at least around the normal maximum is below ± 200 K. For
548 times closer than 100 μs to CZ, where the emission coefficient of the O I triplet could be evaluated by
549 absolute intensity calibration only, the uncertainty depends on the rise of line emission coefficient with
550 temperature. For temperatures below 11 000 K, the emission coefficient is possibly underestimated by
551 factor 2 in maximum, which causes and underestimation of temperature by 900 K.

552 It has been found that the arc was rather broad at 1 000 μs and 400 μs before CZ in agreement with
553 the observations of wall-stabilization. In the following, arc constriction was observed. Despite the
554 uncertainties discussed above, it can be stated that the maximum temperature decreases from above
555 18 000 K at 300 μs to about 11 000 K at 10 μs before CZ.

556 5. Conclusions

557 The main challenge concerning optical investigations of ablation-dominated high-current arcs
558 close to current zero is a low intensity of the emitted radiation. Therefore, different techniques of
559 high-speed camera (HSC) imaging with or without filtering and optical emission spectroscopy (OES)
560 were introduced; their assets and limitations were discussed. It was shown that some important effects
561 can be analyzed even with rather simple nozzle experiments, applicable to other groups and setups.

Two setups were used: With the first setup, experiments with a long, tubular nozzle were applied on to study the CZ transition including new re-ignition of the arc. Using OES with HSC, a dark period of 200 μs around CZ was observed and the differences in spectra before and after CZ were discussed. Radial temperature profiles could be obtained until 400 μs before CZ. Here, a typical case of a well-established arc was found with a broad temperature profile, characteristically for an arc stabilized by ablation of the nozzle wall.

As second setup, a model circuit chamber in CO_2 atmosphere was used to study more realistic, praxis relevant features including flow reversal, arc behavior around CZ, and arc before vanishing. Using OES with intensified CCD camera, higher sensitivity was realized allowing determination of temperature profiles. Whereas ionic carbon lines were applied mainly for quantitative characterization at higher temperatures until 100 μs , atomic oxygen lines delivered quantitative profiles until few microseconds before CZ with higher sensitivity at lower temperatures. Generally, a transition was observed in the arc behavior. Until several hundred microseconds before CZ, the arc was wall-stabilized with broad and rather flat temperature profile. After vanishing of wall stabilization and inflow of cold gas, a highly dynamic arc appeared that was constricted and asymmetric moving out of center. During the transition, the maximum temperatures in the core increased to yield higher current densities for the constricted arc.

In future work it will be important to combine the experimental results and modeling concerning temperature profiles, composition calculation for a determination of current density.

Author Contributions: Conceptualization, R.M. and D.U.; methodology, validation, and formal analysis, R.M.; investigation with setup (a), R.M. and A.K.; investigation with setup (b), R.M., A.K., and N.G.; writing—original draft preparation, R.M. and D.U.; project administration, D.U. All authors have read and agreed to the published version of the manuscript.

Funding: This research was funded by Deutsche Forschungsgemeinschaft grant numbers UH 106/13-1 and SCHN 728/16-1.

Acknowledgments: The authors would like to thank Steffen Franke for experimental help and fruitful discussions. The calculation of plasma composition was realized by Sergey Gortschakow (all Leibniz Institute for Plasma Science and Technology).

Conflicts of Interest: The authors declare no conflict of interest. The funders had no role in the design of the study; in the collection, analyses, or interpretation of data; in the writing of the manuscript, or in the decision to publish the results.

Abbreviations

The following abbreviations are used in this manuscript:

CO_2	carbon dioxide
CZ	current zero
DFO	double frame optics
ICCD	intensified charge coupled device
HSC	high-speed camera
MoS_2	molybdenum disulfide
LTE	local thermal equilibrium
OES	optical emission spectroscopy
PTFE	polytetrafluoroethylene
SF_6	sulfur hexafluoride
W-Cu	tungsten-copper

References

- Seeger, M. Future Perspectives on High Voltage Circuit Breaker Research. *Plasma Phys. Technol.* **2015**, *2*, 271–279.
- Seeger, M. Perspectives on research on high voltage gas circuit breakers. *Plasma Chemistry and Plasma Processing* **2015**, *35*, 527–541.

- 602 3. Glaubitz, P.; Stangherlin, S.; Biasse, J.; Meyer, F.; Dallet, M.; Pruefert, M.; Kurte, R.; Saida, T.; Uehara,
603 K.; Prieur, P.; Ito, H.; Kynast, E.; Janssen, A.; Smeets, R.; Dufournet, D. CIGRE position paper on the
604 application of SF₆ in transmission and distribution networks. *Electra* **2014**, *34*, 34–39.
- 605 4. Christophorou, L.; Olthoff, J.K.; Green, D.S. Gases for electrical insulation and arc interruption: Possible
606 present and future alternatives to pure SF₆. *NIST Technical Note 1425* **1997**, *Nov.*, 1–44.
- 607 5. Robin-Jouan, P.; Bousoltane, K.; Kieffel, Y.; Trepanier, J.Y.; Camarero, R.; Arabi, S.; Pernaumat, G. Analysis
608 of last development results for high voltage circuit-breakers using new g³ gas. *Plasma Phys. Technol.* **2000**,
609 *33*, 2583–2590.
- 610 6. Godin, D.; Trepanier, J.Y.; Reggio, M.; Zhang, X.D.; Camarero, R. Modelling and simulation of nozzle
611 ablation in high-voltage circuit-breakers. *J. Phys. D Appl. Phys.* **2000**, *33*, 2583–2590.
- 612 7. Wu, Y.; Wang, C.; Sun, H.; Murphy, A.B.; Rong, M.; Yang, F.; Chen, Z.; Niu, C.; Wang, X. Properties of
613 C₄F₇N–CO₂ thermal plasmas: thermodynamic properties, transport coefficients and emission coefficients.
614 *J. Phys. D: Appl. Phys.* **2007**, *51*, 155206.
- 615 8. Seeger, M.; Smeets, R.; Yan, J.; Ito, H.; Claessens, M.; Dullni, E.; Falkingham, L.; Franck, C.M.; Gentils, F.;
616 Hartmann, W.; Kieffel, Y.; Jia, S.; Jones, G.; Mantilla, J.; Pawar, S.; Rabie, M.; Robin-Jouan, P.; Schellekens,
617 H.; Spencer, J.; Uchii, T.; Li, X.; Yanabu, S. Recent Trends in Development of High Voltage Circuit Breakers
618 with SF₆ Alternative Gases. *Plasma Phys. Technol.* **2017**, *4*, 8–12.
- 619 9. Stoller, P.C.; Seeger, M.; Iordanidis, A.A.; Naidis, G.V. CO₂ as an arc interruption medium in gas circuit
620 breakers. *IEEE Trans. Plasma Sci.* **2013**, *41*, 2359–2369.
- 621 10. Guo, Z.; Liu, S.; Pu, Y.; Zhang, B.; Li, X.; Tang, F.; Lv, Q.; Jia, S. Study of the arc interruption performance of
622 CO₂ gas in high-voltage circuit breaker. *IEEE Trans. Plasma Sci.* **2019**, *47*, 2742–2751.
- 623 11. Kozakov, R.; Kettlitz, M.; Weltmann, K.D.; Steffens, A.; Franck, C.M. Temperature profiles of an ablation
624 controlled arc in PTFE: I. Spectroscopic measurements. *J. Phys. D: Appl. Phys.* **2007**, *40*, 2499–2506.
- 625 12. Methling, R.; Franke, S.; Uhrlandt, D.; Gorchakov, S.; Reichert, F.; Petchanka, A. Spectroscopic Study of
626 Arc Temperature Profiles of a Switching-off Process in a Model Chamber. *Plasma Phys. Technol.* **2015**,
627 *2*, 163–166.
- 628 13. Ruchti, C.B.; Niemeyer, L. Ablation controlled arcs. *IEEE Trans. Plasma Sci.* **1986**, *14*, 423–434.
- 629 14. Bort, L.; Schultz, T.; Franck, C.F. Determining the time constant of arcs at arbitrary current levels. *Plasma*
630 *Phys. Technol.* **2019**, *5*, 175–179.
- 631 15. Schultz, T.; Hammerich, B.; Bort, L.; Franck, C.F. Improving interruption performance of mechanical circuit
632 breakers by controlling pre-current-zero wave shape. *High Voltage* **2019**, *4*, 122–129.
- 633 16. Methling, R.; Khakpour, A.; Wetzeler, S.; Uhrlandt, D. Investigation of an ablation-dominated arc in a
634 model chamber by optical emission spectroscopy. *Plasma Phys. Technol.* **2017**, *4*, 153–156.
- 635 17. Eichhoff, D.; Kurz, A.; Kozakov, R.; Gött, G.; Uhrlandt, D.; Schnettler, A. Study of an ablation-dominated
636 arc in a model circuit chamber. *J. Phys. D: Appl. Phys.* **2012**, *45*, 305204.
- 637 18. Seeger, M.; Tepper, J.; Christen, T.; Abrahamson, J. Experimental study on PTFE ablation in high voltage
638 circuit-breakers. *J. Phys. D: Appl. Phys.* **2006**, *39*, 5016–5024.
- 639 19. Seeger, M.; Niemeyer, L.; Christen, T.; Schwinne, M.; Dommerque, R. An integral arc model for ablation
640 controlled arcs based on CFD simulations. *J. Phys. D: Appl. Phys.* **2006**, *39*, 2180–2191.
- 641 20. Methling, R.; Götte, N.; Uhrlandt, D. Ablation-Dominated Arcs in CO₂ atmosphere - Part II: Molecule
642 emission and absorption.
- 643 21. Kramida, A.; Ralchenko, Y.; Reader, J.; Team, N.A. NIST Atomic Spectra Database (version 5.7.1). [Online].
644 Available: <http://physics.nist.gov/asd> [retrieved January 2020], National Institute of Standards and
645 Technology, Gaithersburg, Maryland, 2019.
- 646 22. Kurucz, R.L.; Bell, B. Atomic Line Data. Kurucz CD-ROM No. 23. [Online].
647 Available: <http://www.cfa.harvard.edu/amp/ampdata/kurucz23/sekur.html> [retrieved December 2011],
648 Smithsonian Astrophysical Observatory, 1995.
- 649 23. Methling, R.; Franke, S.; Uhrlandt, D.; Gorchakov, S.; Panousis, E. Spectroscopic measurements of arc
650 temperatures in a model HV circuit breaker. *Plasma Phys. Technol.* **2015**, *2*, 163–166.